

Stable and Bright Electroluminescent Devices utilizing Emissive 0D Perovskite Nanocrystals Incorporated in a 3D CsPbBr₃ Matrix

Aditya Mishra, Riya Bose, Yangzi Zheng, Weijie Xu, Reema McMullen, Abhas B. Mehta, Moon J. Kim, Julia W. P. Hsu, Anton V. Malko, and Jason D. Slinker*

The 0D cesium lead halide perovskite Cs₄PbBr₆ has drawn remarkable interest due to its highly efficient robust green emission compared to its 3D CsPbBr₃ counterpart. However, seizing the advantages of the superior photoluminescence properties for practical light-emitting devices remains elusive. To date, Cs₄PbBr₆ has been employed only as a higher-bandgap nonluminescent matrix to passivate or provide quantum/dielectric confinement to CsPbBr₃ in light-emitting devices and to enhance its photo-/thermal/environmental stability. To resolve this disparity, a novel solvent engineering method to incorporate highly luminescent 0D Cs₄PbBr₆ nanocrystals (perovskite nanocrystals (PNCs)) into a 3D CsPbBr₃ film, forming the active emissive layer in single-layer perovskite light-emitting electrochemical cells (PeLECs) is designed. A dramatic increase of the maximum external quantum efficiency and luminance from 2.7% and 6050 cd m⁻² for a 3D-only PeLEC to 8.3% and 11 200 cd m⁻² for a 3D–0D PNC device with only 7% by weight of 0D PNCs is observed. The majority of this increase is driven by the efficient inherent emission of the 0D PNCs, while the concomitant morphology improvement also contributes to reduced leakage current, reduced hysteresis, and enhanced operational lifetime (half-life of 129 h), making this one of the best-performing LECs reported to date.

long carrier diffusion lengths, and defect tolerance, leading to skyrocketing performance in thin-film optoelectronics.^[1] Compared to hybrid organic–inorganic perovskites, inorganic perovskites offer improved chemical and thermal stability while retaining most of the advantageous properties. In particular, cesium lead halide perovskites (CsPbX₃, X = Cl, Br, I) have gained significant attention for light-emitting applications because of their high photoluminescence (PL) quantum yield (QY), color-purity, widely tunable emission, and facile solution processability.^[2] Recently, green perovskite light-emitting diodes (LEDs) have achieved impressive external quantum efficiencies (EQEs) approaching and exceeding ≈20%.^[3] However, CsPbX₃ light-emitting devices still suffer from fast excitonic decay due to weakly bound excitons that can be easily thermally dissociated and diffused with lattice vibration, thereby being trapped by nonradiative defect states, which arise due to their labile surface as well as environmental factors.^[4] This rapid excitonic decay

renders the PLQY sensitive to the material form and requires additional defect passivation/encapsulation strategies such as embedding in polymer additives, incorporating dopants, and engineering ligand shells to circumvent this issue.^[4a,5]


Contrary to the 3D perovskites CsPbX₃, where the [PbX₆]⁴⁻ octahedra are corner shared along all three dimensions, isolation of octahedra in 0D Cs₄PbX₆ leads to a higher exciton binding energy and, consequently, a remarkable enhancement of PL intensity that remains in the solid-state along with superior environmental stability.^[6] The origin of the emission in 0D perovskites, which spectrally is nearly identical to the 3D perovskites despite the higher bandgap of the former, has often been assigned to the embedded 3D impurities.^[7] However, several studies have ruled out the presence of 3D impurities by intensive structural characterization and attributed the origin of the emission to the presence of molecular-like intrabandgap defects.^[6a,8] In particular, 0D Cs₄PbBr₆ has been extensively studied from both theoretical and experimental aspects, and it has been observed that Br vacancies (V_{Br}) in 0D Cs₄PbBr₆ have a low formation energy and can induce a mid-gap energy

1. Introduction

In recent years, lead halide perovskites have been the community's choice material, exhibiting high absorption coefficients,

A. Mishra, W. Xu, A. B. Mehta, M. J. Kim, J. W. P. Hsu, J. D. Slinker
 Department of Materials Science and Engineering
 The University of Texas at Dallas
 800 West Campbell Rd., Richardson, TX 75080-3021, USA
 E-mail: slinker@utdallas.edu

R. Bose, Y. Zheng, R. McMullen, A. V. Malko, J. D. Slinker
 Department of Physics
 The University of Texas at Dallas
 800 West Campbell Rd., Richardson, TX 75080-3021, USA
 J. D. Slinker
 Department of Chemistry
 The University of Texas at Dallas
 800 West Campbell Rd., Richardson, TX 75080-3021, USA

 The ORCID identification number(s) for the author(s) of this article can be found under <https://doi.org/10.1002/adma.202203226>.

DOI: 10.1002/adma.202203226

level appropriate to achieve the green emission.^[9] Thus, there is considerable literature evidence demonstrating emission from 0D Cs_4PbBr_6 (Table S1, Supporting Information).^[6a,8,9] Notably, non-emissive Cs_4PbBr_6 has found widespread application as a matrix to encapsulate CsPbBr_3 , as it can passivate the surface by endotaxy without any resulting strain.^[10] Such a nonluminescent 0D phase restricts the growth of CsPbBr_3 crystallites, leading to increased confinement and enhancement of exciton binding energy.^[11] Cs_4PbBr_6 , being a higher bandgap material, can also provide type-I confinement to CsPbBr_3 , thereby restricting the carriers within the CsPbBr_3 region and reducing the probability of electron leakage,^[12] or can provide dielectric confinement to the 3D part, enhancing its oscillator strength and absorption cross-section.^[13] Energy transfer from the 0D to 3D has also been reported.^[14] Overall, reducing non-radiative losses and facilitating radiative recombination significantly enhance the EQE of CsPbBr_3 light-emitting devices. Additionally, it also improves the photo, thermal, and environmental stability of the devices, resulting in longer operational lifetimes.^[11b,15]

Surprisingly, regardless of all the efforts to identify the origin of the emission from 0D Cs_4PbBr_6 , much less has been done to implement its propitious emission properties in light-emitting devices, with limited reports of using them for luminescent solar concentrators, white LEDs, lasing, and X-ray scintillators.^[16] Here, we designed a novel solvent engineering method to incorporate highly emissive 0D perovskite nanocrystals

(PNCs) into a 3D perovskite composite film (CsPbBr_3 , a polyelectrolyte, and Li salt) to form the emissive layer in single-layer perovskite light-emitting electrochemical cells (PeLECs).^[17] LECs utilize mobile ion redistribution to enhance charge injection and produce efficient emission from solution processible single-layer devices.^[18] It is observed that incorporation of an optimized concentration of highly luminescent (PLQY $\approx 70\%$) 0D PNCs in a CsPbBr_3 matrix can dramatically improve virtually all of the PeLEC optoelectronic properties. In particular, PeLECs utilizing these highly emissive 0D PNCs exhibit a maximum luminance of $11\,200\text{ cd m}^{-2}$, a maximum power efficiency of 33.0 lm W^{-1} , a maximum EQE of 8.3%, and a long luminescence half-life of 129 h when operated at 10 mA cm^{-2} . The rationale for this enhancement is established by a detailed analysis of the PL and electroluminescence (EL) of various film and device formulations coupled with morphological and structural evaluation by microscopy and diffraction.

2. Results and Discussion

2.1. Fabrication and PL of 3D–0D Blended Films

Figure 1a presents our method to fabricate 3D–0D PNC LECs. Since the morphology of the film is a crucial component to ensure optimum device performance, our major challenge was to distribute the 0D PNCs into the 3D matrix while retaining its

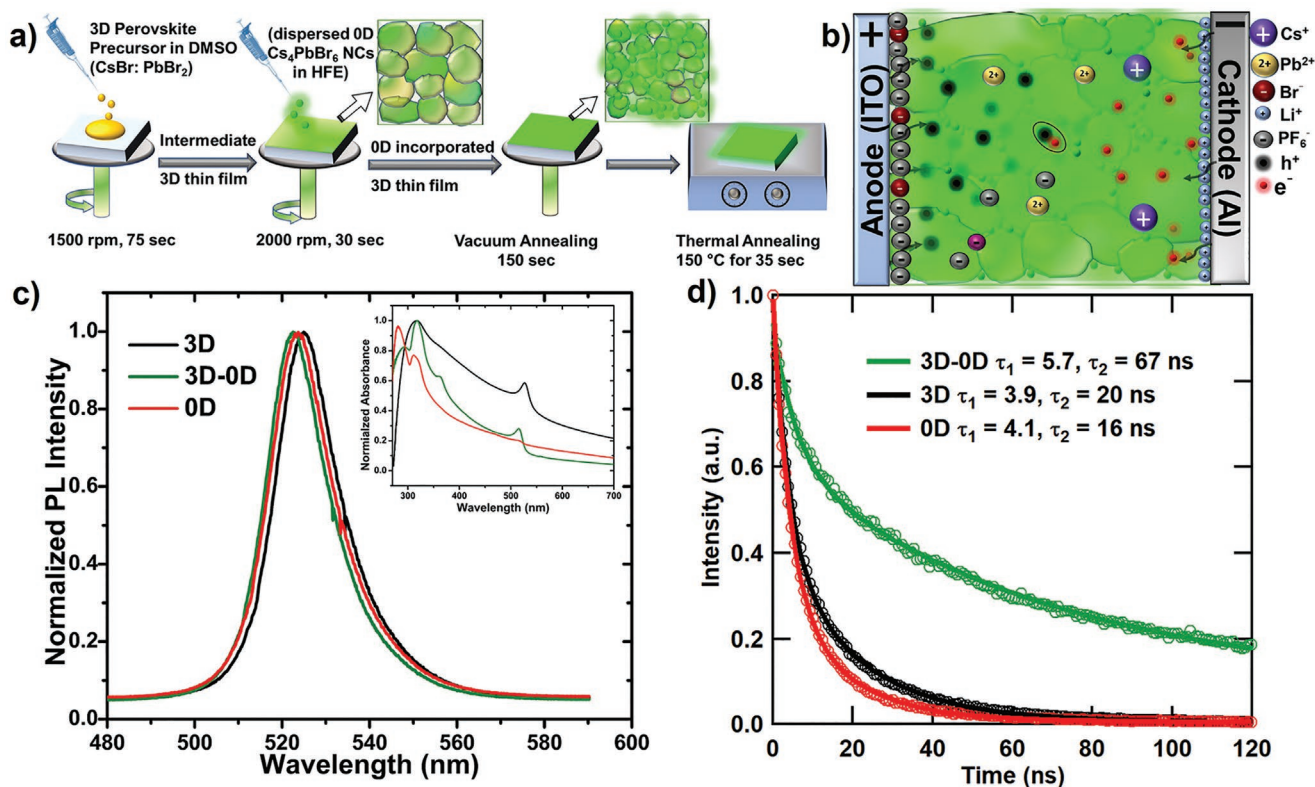


Figure 1. Fabrication method and PL from thin films of 0D and 3D perovskite blends. a) Illustration of the fabrication method for dispersing 0D PNCs in a 3D matrix. b) Illustration of the ionic redistribution and charge dynamics in PeLECs. c) Normalized steady-state PL spectra of 0D, 3D, and 3D–0D perovskite composite thin films. (Inset: Absorbance spectra of 0D, 3D, and 3D–0D perovskite composite thin films.) d) Normalized time-resolved PL spectra of 0D, 3D, and 3D–0D perovskite composite thin films.

crystal structure network. To achieve this, we modified our previously reported procedure used to fabricate standard 3D PeLECs. Typically, a precursor solution of the 3D CsPbBr₃ (CsBr:PbBr₂, mixing ratio of 1.5:1), poly(ethylene oxide) electrolyte, and LiPF₆ salt additive was spin-cast from dimethyl sulfoxide (DMSO) solution onto glass slides bearing the modified bottom electrode of indium tin oxide (ITO)/poly(3,4-ethylenedioxythiophene)-polystyrene sulfonate (PEDOT-PSS). Selective addition of poly-electrolyte and salt of highly mobile ions is advantageous to attain differentiated ion motion in PeLECs and maintain the perovskite ionic crystal,^[17c,e,f] as illustrated in Figure 1b. Once this film was set, presynthesized 0D Cs₄PbBr₆ PNCs (synthesized following a literature-reported procedure^[9c]) in different weight ratios were introduced utilizing a hydrofluoroether (HFE) “orthogonal solvent,” a solvent that selectively suspends the 0D PNCs while maintaining the underlying structure of the film (Figure S1 and Table S2, Supporting Information).^[19] (Notably, the long-chain ligands present on 0D PNCs prohibit using them as the sole emitters in PeLECs.) The utility of HFE to nondestructively interact with 3D perovskite films has been previously established.^[19b] Afterward, the film was annealed in vacuum and at 150 °C to set the crystal structure of the film.

Figure 1c shows the steady-state absorption (inset) and emission spectra of the individual 3D, 0D PNCs (70% PLQY), and the 3D–0D PNCs composite films. While the absorption spectrum of the composite shows collective features of both 3D and 0D, the emission spectrum reveals an emission peak of similar full-width at half-maximum centered at 523 nm, which is slightly blueshifted compared to 3D (\approx 525 nm) and 0D (\approx 524 nm)

components. However, the PL lifetime (Figure 1d) of the composite emission is significantly elongated compared to either 3D or 0D films, implying reduction of fast carrier-trapping channels.

2.2. 3D–0D PNC PeLECs

Since the 3D–0D PNCs blend showed a clear improvement of the PL properties over the 3D counterpart, we compared their EL performances as the active material in PeLECs with an ITO/PEDOT-PSS/perovskite:PEO:LiPF₆/LiF/Al architecture. To further investigate how the intrinsic PL qualities of 0D PNCs affect the overall emission from the composite device, we employed emissive 0D PNCs with high (\approx 70%) and low (\approx 30%) PLQY, as well as non-emissive 0D PNCs synthesized per literature-reported procedures.^[7b,9d] Figure 2a shows the EL spectra of 3D and 3D–0D PNCs PeLECs with 0D PNCs of various PLQY under 4.5 V bias. The 3D films exhibit a narrow EL emission peak centered at 522 nm, characteristic of CsPbBr₃ PeLECs,^[17b–d] whereas 3D–0D PNCs composites exhibit slightly blueshifted emission centered at 518 nm, similar to the blueshift observed in the PL. EL spectra featuring similar characteristics as PL indicate a minimal impact of the fabrication process on the integrity of the perovskite thin film. However, the EL intensities of the composites with emissive 0D PNCs are significantly higher than that of the 3D-only device, with the high PLQY composite producing an approximately threefold enhancement of the maximum. By contrast, the 3D–0D composite with non-emissive 0D PNCs has a lower EL intensity than the 3D-only device.

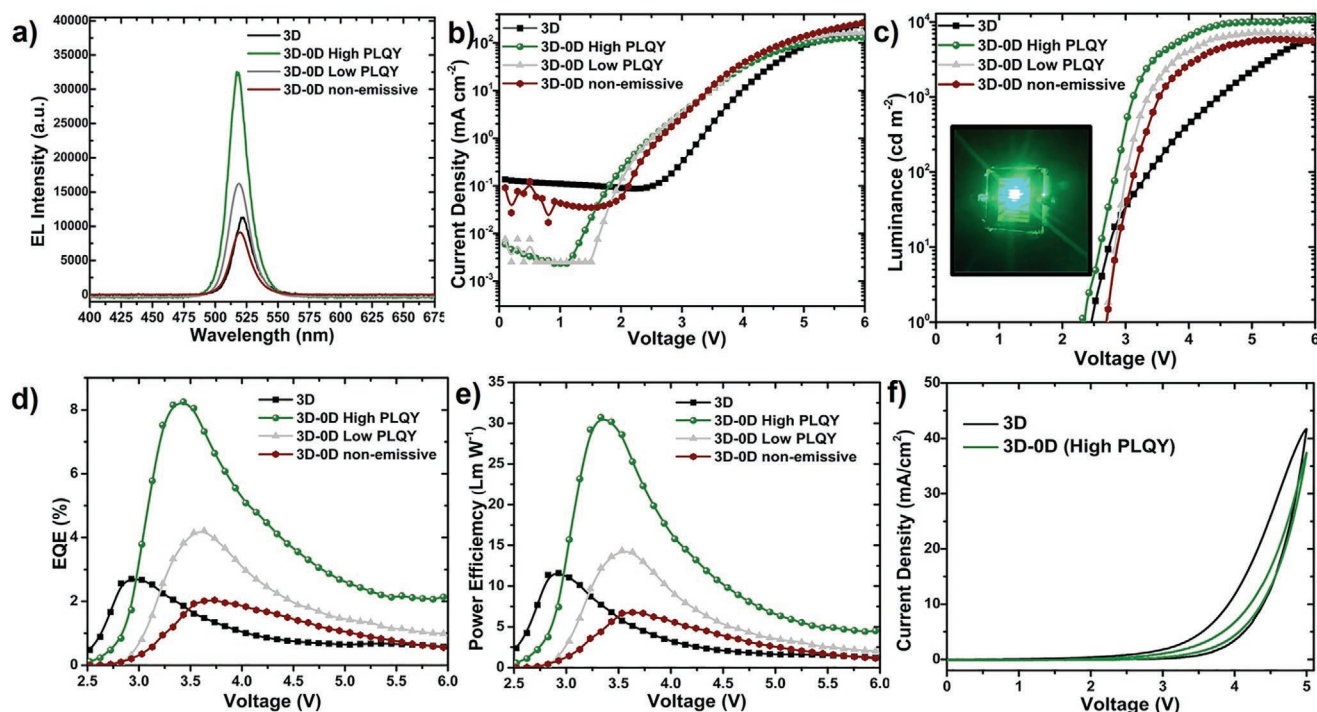


Figure 2. EL spectra and luminance–current–voltage characteristics of 3D and 3D–0D PeLECs. a) EL spectra of 3D and 3D–0D PeLECs at 4.5 V. b) Current density versus voltage for 3D and 3D–0D PeLECs. c) Luminance versus voltage for 3D and 3D–0D PeLECs. (Inset: Operation of a 3D–0D (high PLQY) PeLEC at 4.5 V.) d) EQE versus voltage for 3D and 3D–0D PeLECs. e) Power efficiency versus voltage for 3D and 3D–0D PeLECs. f) Current density versus voltage sweeps for 3D and 3D–0D PeLECs.

The current densities of the 3D and 3D–0D PeLECs from current/voltage sweeping from 0 to 6 V are presented in Figure 2b. The redistribution of ions largely dictates current injection in single-layer LECs, and the thin-film quality governs background/leakage current. The 3D device exhibits significant leakage current ($\approx 0.1 \text{ mA cm}^{-2}$) at low voltages and an onset of significant current injection above this threshold near 2.8 V. Adding the 0D PNCs lowers the leakage current density, with the 3D–0D (low PLQY) PeLEC and the 3D–0D (high PLQY) decreasing leakage current by an order of magnitude. Furthermore, the onset of current injection above this threshold is lowered to 2.0 V for the 3D–0D (non-emissive) PeLEC, 1.6 V for the 3D–0D (low PLQY) PeLEC, and 1.3 V for the 3D–0D (high PLQY) PeLEC. This lowered injection voltage threshold suggests that the 0D PNCs help facilitate ionic transport, potentially through the passivation of trapping channels from the 3D perovskite lattice, as evidenced from time-resolved PL.

Figure 2c shows the luminance of the PeLECs from current/voltage sweeping from 0 to 6 V. The onset of luminance above 1 cd m^{-2} , characteristic of the injection of the minority carrier, is observed between 2.3 and 2.7 V for these devices, with the 3D–0D (high PLQY) sample possessing the lowest onset voltage threshold. Likewise, the voltage to surpass 100 cd m^{-2} luminance lowers from 3.4 V for the 3D-only PeLEC to 2.9 V for the 3D–0D (high PLQY) device. Over this 6 V range, the 3D device peaks at a luminance of 6050 cd m^{-2} , the 3D–0D (non-emissive) PeLEC at 5800 cd m^{-2} , the 3D–0D (low PLQY) PeLEC at 7300 cd m^{-2} , and the 3D–0D (high PLQY) at $11\,200 \text{ cd m}^{-2}$. (See Figure S2, Supporting Information, for a statistical comparison of luminance maxima.) Thus, incorporating either low or high PLQY 0D PNCs to 3D film leads to higher peak luminance, whereas the non-emissive 0D lowers peak luminance. In addition, while the low PLQY 0D insertion improves this metric by only $\approx 20\%$, the high PLQY 0D PNCs raise the luminance by 85%. This differential enhancement unequivocally indicates that the intrinsic emission quality of the 0D PNCs is the prime factor enhancing the luminance of the composite PeLECs.

To further understand how 0D PNCs impact PeLEC performance, the efficiency metrics from these devices are shown in Figure 2d,e. The EQE of the 3D-only PeLEC peaks at 2.7% photons per electron, as seen in Figure 2d. The addition of the low PLQY 0D PNCs raises this peak EQE to 4.2%, while the high PLQY device maximizes at 8.3%, among the best values reported for single-layer LECs.^[20] Alternatively, the 3D–0D (non-emissive) PeLEC decreases the peak EQE to 2.0%, and likewise decreases other efficiency metrics (Table S2, Supporting Information). (See Figure S2, Supporting Information, for a statistical comparison of EQE maxima.) The power efficiency maximum improves from 11.6 lm W^{-1} for the 3D-only PeLEC, to 14.3 lm W^{-1} for the 3D–0D (low PLQY) PeLEC, and to 33.0 lm W^{-1} for the 3D–0D (high PLQY) PeLEC. Again, this 33.0 lm W^{-1} measure is among the best reported for single-layer LECs.^[20] What is more, these efficiency metrics are achieved at 3070 cd m^{-2} for the 3D–0D (high PLQY) PeLEC. Thus, the inclusion of emissive 0D PNCs into a 3D perovskite matrix greatly enhances quantum and power efficiency metrics, with the 3D–0D (high PLQY) PeLEC rivaling the best performance in the field for single-layer LECs. Furthermore, while the low

PLQY 0D PNCs improve the efficiency over 3D-only devices by $\approx 25\text{--}55\%$, introducing the high PLQY 0D PNCs into the film doubles and triples the EQE and power efficiency, respectively. Again, these metrics demonstrate that the efficiency of the 0D PNC emission determines the efficiency of 3D–0D blended PeLECs.

In addition, blending the 0D PNCs into the 3D matrix reduces the hysteresis associated with cyclic PeLEC operation. Hysteresis in LECs occurs from slow ion relaxation. Figure 2f shows the plot from cyclic current–voltage sweeping of 3D and 3D–0D high PLQY PeLECs. The hysteresis in current is greatly reduced, indicating more efficient ion transport with the inclusion of the 0D PNCs.

To assess the impact of emissive 0D PNCs on the stability of the PeLECs, the devices were operated at constant current, with the data presented in Figure 3a,b. One general metric is the luminance half-life, the time to decay from the maximum to half-maximum. Under 33.3 mA cm^{-2} operation, the 3D PeLEC achieves a 3120 cd m^{-2} luminance maximum and exhibits a luminance half-life of 26.0 h. Likewise, under 33.3 mA cm^{-2} operation, the 3D–0D (high PLQY) PeLEC achieves a 3640 cd m^{-2} luminance maximum and exhibits a luminance half-life of 46.2 h, highly competitive among PeLEC devices (Table S3, Supporting Information). As lifetimes of PeLECs generally scale inversely with luminance as a power law, we also ran the 3D–0D (high PLQY) PeLEC at a constant current density of 10 mA cm^{-2} to observe longer lifetimes. For this experiment, the PeLEC peaked at a luminance maximum of 1530 cd m^{-2} and yielded a half-life of 129 h, among the best for perovskite light-emitting devices (Table S3, Supporting Information).^[3a,5i,17c,21] This lifetime enhancement is likely owed to the passivation of the 3D perovskite matrix by stable and emissive 0D PNCs and the preservation of the perovskite lattice by differentiated ion motion in the PeLEC—selective redistribution of the LiPF_6 additive ions.

In Figure 3b, the operational voltage for each device under constant current is plotted. Constant current generally induces a higher voltage in the initial stages of operation while the device is resistive, encouraging facile ionic redistribution. On longer timescales, the voltage lowers as ion accumulation at the electrodes increases charge injection and lowers device resistance. For the 3D PeLEC at 33.3 mA cm^{-2} constant current, after beginning near 4 V, the steady-state voltage ranges from 3.0 to 3.4 V. The 3D–0D PeLEC at 33.3 mA cm^{-2} also initiates near 4 V, but the voltage quickly lowers to operate at a low 2.5–2.7 V. This suggests that the 0D PNCs improve the conductivity of the overall device, and, given the observations from I – V testing, this improvement may originate from more facile ionic redistribution enhancing injection and carrier density. At 10.0 mA cm^{-2} , the 3D–0D PeLEC achieves an even lower steady-state voltage of 2.3 V, approaching the bandgap of these perovskites.

The mounting evidence of improved ionic redistribution and electronic conductivity from 0D emissive PNC inclusion led us to investigate the phenomenon by electrochemical impedance spectroscopy and fitting with an equivalent circuit model. The complex impedance for 3D and 3D–0D PeLECs is plotted as the magnitude and phase angle versus frequency in Figure 3c,d, respectively. The equivalent circuit model used to fit the curve

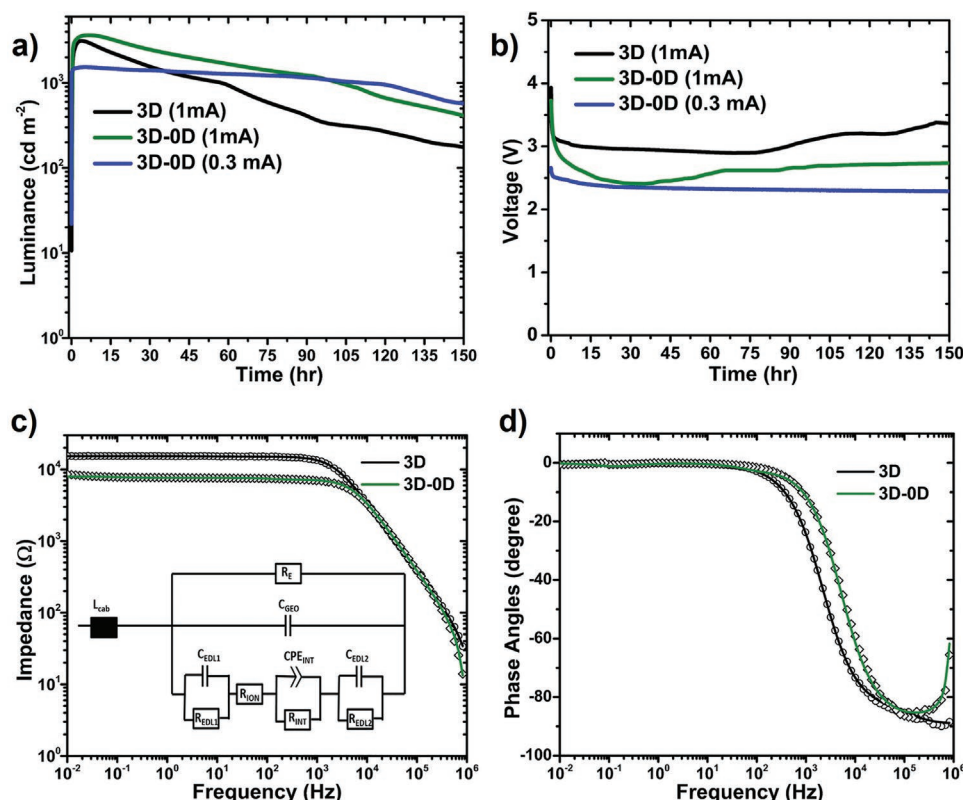


Figure 3. Constant current density and electrochemical impedance characteristics of 3D and 3D-0D (high PLQY) PeLECs. a) Luminance vs time for 3D and 3D-0D (high PLQY) PeLECs at 33.3 mA cm^{-2} and a 3D-0D (high PLQY) PeLEC at 10 mA cm^{-2} constant current density. b) Voltage vs time for 3D and 3D-0D (high PLQY) PeLECs at 33.3 mA cm^{-2} and a 3D-0D (high PLQY) PeLEC at 10 mA cm^{-2} constant current density. c) Complex impedance magnitude versus frequency for 3D and 3D-0D (high PLQY) PeLECs. The solid lines are equivalent circuit fits to the data. (Inset: equivalent circuit model.) d) Complex impedance phase angle versus frequency for 3D and 3D-0D (high PLQY) PeLECs. The solid lines are equivalent circuit fits to the data.

is shown as the inset in Figure 3c, a model that has previously fitted PeLEC operation.^[17c] At low frequencies ($<1 \text{ kHz}$), the 3D-0D PeLEC exhibits a lower impedance than the 3D counterpart (Figure 3c). The corner frequency increases from 2 kHz for the 3D PeLEC to 10 kHz for the 3D-0D PeLEC, a substantial improvement consistent with a greater ionic (capacitive) response. Similarly, the trend toward higher phase angles and more complex behavior is shifted to higher frequencies for the 3D-0D blend in Figure 3d.

The equivalent circuit model provides an excellent fit to the impedance curves (solid lines of Figure 3c,d), and the parameters extracted from this fitting according to previously discussed methods^[17c,22] are shown in Table 1. In short, this equivalent circuit accounts for an overall resistance, an overall geometric capacitance, double layer formation at each contact with a resistor and capacitor in parallel, and internal ionic effects. The conductivity of the 3D-0D device is 75% higher than the

3D-only PeLEC analog. The dielectric constant is reduced from 15.3 for the 3D PeLEC to 10.8 for the 3D-0D blend, consistent with the strongly bound excitons of the 0D component^[6,9c] and beneficial for enhanced luminance, as Langevin recombination is inversely proportional to the dielectric constant.^[22b] Concerning double layer formation, the capacitance increases with the 3D-0D blend, and the widths are decreased by $\approx 40\%$ relative to the 3D device to 3.0 and 3.3 nm. The thinner widths are ideal for a narrower tunnel barrier for charge injection at each contact, and the symmetric barrier widths assist balanced injection for high recombination efficiency. The geometric capacitance decreases for the 3D-0D device, consistent with a greater participation of ions in double-layer formation. Hence, electrochemical impedance spectroscopy affirms the beneficial effects of 0D emissive PNC incorporation in the 3D matrix on electrical and ionic transport in PeLECs and additional factors that improve emission efficiency.

Table 1. Equivalent circuit and thin-film parameters extracted from electrochemical impedance spectroscopy analysis of 3D and 3D-0D (high PLQY) PeLECs.

Sample	Thickness [nm]	$C_{\text{GEO}}^{\text{a)}$ [nF]	Dielectric constant	$C_{\text{EDL1}}^{\text{b)}$ [nF]	$C_{\text{EDL2}}^{\text{c)}$ [nF]	$W_{\text{EDL1}}^{\text{d)}$ [nm]	$W_{\text{EDL2}}^{\text{e)}$ [nm]	Conductivity ^{f)} [$\mu\text{S m}^{-1}$]
3D	125	3.25	15.3	83	71	4.9	5.7	84.7
3D-0D	125	2.31	10.8	96	85	3.0	3.3	148

^{a)}Geometric capacitance; ^{b)}Capacitance of EDL 1; ^{c)}Capacitance of EDL 2; ^{d)}Width of EDL 1; ^{e)}Width of EDL 2; ^{f)}Electrical conductivity.

2.3. Structural Characterization of 3D and 3D–0D Perovskite Thin Films

It is important to physically characterize the thin-film properties to ascertain if morphological effects also contribute to the superior performance of the 3D–0D emissive PNCs blends and verify the presence of each component. Notably, high-resolution transmission electron microscopy (HRTEM) and fast Fourier transform analysis of 0D PNCs (high PLQY) confirm Cs_4PbBr_6 lattice planes^[9d] and absence of any 3D impurity (Figure S3, Supporting Information). Alternative to these emissive PNCs, all the previous reports of 3D–0D composites or light-emitting devices incorporating a non-emissive 0D component involved changing the CsBr to PbBr_2 precursor ratio, where increasing the CsBr ratio led to more 0D phase formation, which in turn reduced the crystallite/grain size of the 3D part leading to

increased confinement.^[10b,14b,23] To compare our 3D–0D PNC blend with those from literature reports, we prepared composite films with an excess of CsBr ($\text{CsBr}:\text{PbBr}_2 = 2:1$ and $3:1$) and analyzed the structural details and device performance relative to the 3D and 3D–0D (high PLQY) PNC composite. As can be seen from the scanning electron microscopy (SEM) images provided in Figure 4a, the introduction of 0D (high PLQY) PNCs reduces the grain size significantly compared to the 3D film ($\text{CsBr}:\text{PbBr}_2 = 1.5:1$). In addition, both the 3D–0D film and the $3:1$ precursor film showed a bimodal size distribution, while the 3D film was monomodal (Figure 4b). However, the films appeared smoothest and having the fewest pinholes for the 3D–0D film. This assertion can be further confirmed from the atomic force microscopy (AFM) images provided in Figure 4c. The incorporation of 0D PNCs reduces the surface roughness almost twofold, from 15 to 8.0 nm compared to 3D

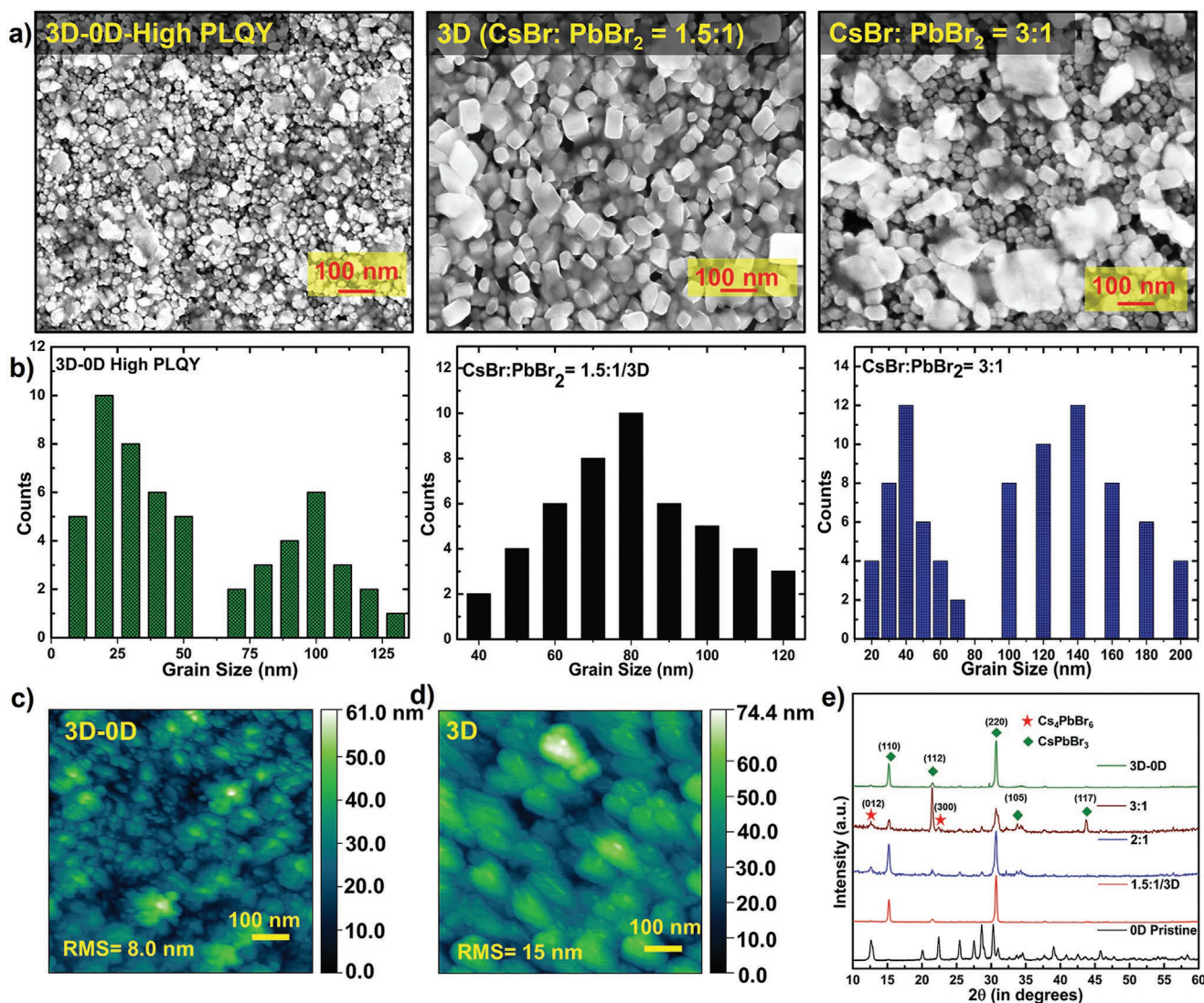


Figure 4. a) SEM of thin films of 3D–0D (high PLQY) perovskites, as well as the 3D-only ($\text{CsBr}:\text{PbBr}_2 = 1.5:1$) film and a film cast from a different precursor ratio ($\text{CsBr}:\text{PbBr}_2 = 3:1$) to spontaneously produce the 0D phase in the 3D matrix. Additional SEM images are provided in Figure S4, Supporting Information. b) Size distribution analysis from SEM of various perovskite thin films. c) Atomic force microscopy (AFM) image of a thin film of 3D–0D (high PLQY) perovskites. d) AFM image of a thin 3D perovskite film. e) XRD of thin films of emissive 0D PNCs (high PLQY) and different composite 3D–0D perovskite films, including those from various $\text{CsBr}:\text{PbBr}_2$ precursor ratios.

film (Figure 4c,d). Additionally, the 3D–0D (high PLQY) PNC film shows tighter packing and evidence of fewer pinholes. These features are all beneficial for suppressed leakage current leading to higher quantum efficiencies and greater device reliability. However, since the composites involving high PLQY, low PLQY, and non-emissive 0D PNCs show similar morphology (Figures S4 and S5, Supporting Information), and yet a significant difference in the performance of the corresponding PeLECs, the emission PLQY of the 0D PNCs indeed plays a crucial role along with the change in morphology. It is important to mention here that unlike literature reports where the thin-film morphology is mostly dominated by larger 0D grains which encapsulate/act as a matrix for smaller 3D grains, in our case, only ≈ 7 wt% addition of 0D PNCs compared to 3D implies that the grains we observe in the SEM images are still originating primarily from the 3D part.

To further confirm the ratios between 0D and 3D components, we analyzed the X-ray diffraction (XRD) patterns of the same samples, along with the films prepared by varying CsBr and PbBr₂ ratios. As shown in Figure 4e, the 3D film (CsBr:PbBr₂ = 1.5:1) showed major diffraction peaks at 15.3°, 21.5°, and 30.7°, in agreement with previous reports for an orthorhombic (*Pnma*) crystal structure.^[24] (See Figure S6, Supporting Information for additional XRD patterns.) With an increase in the CsBr:PbBr₂ ratio, the XRD shows an appearance and consecutive increase of characteristic 0D Cs₄PbBr₆ peaks at 12.7° and 22.4° (marked red).^[10b,23] The most intense 0D peaks were observed for CsBr:PbBr₂ ratio of 3:1, indicating an increased amount of 0D component in the composite. However, for the 3D–0D PNC blend, the ratio of 0D peaks relative to 3D remains negligible, which agrees with the presence of a low weight percentage of 0D PNCs relative to 3D.

2.4. 3D–0D PeLECs Fabricated using Different Precursor Ratios

To clarify how incorporating highly emissive 0D PNCs into 3D CsPbBr₃ PeLECs using a novel solvent engineering method dramatically improves the maximum luminance (11 200 cd m⁻²), power efficiency (33.0 lm W⁻¹), and quantum efficiency (8.3%), as well as the operational stability (129 h at 10 mA cm⁻²) of the device. This operational stability is among the best for perovskite electroluminescent devices. It also improves the film morphology by reducing grain size, surface roughness, and the number of pinholes, resulting in suppressed leakage current. Contrary to all the previous reports of light-emitting devices involving 3D CsPbBr₃–0D Cs₄PbBr₆ materials where non-emissive 0D part acts mostly as a surface passivating matrix to provide quantum/dielectric confinement, the high intrinsic luminescence of the 0D PNCs plays a crucial role in significantly enhancing the luminance of our composites. This approach opens numerous

(CsBr:PbBr₂ 1.5:1) with devices prepared from CsBr:PbBr₂ precursor formulations of 2:1 and 3:1 having a significant 0D phase as observed in XRD. These spontaneous 3D–0D films allow us to compare their performance to the 3D–0D devices from pre-synthesized 0D PNCs of low and high PLQY (Figure 2). From the current density versus voltage curve provided in Figure 5a, it is obvious that an increase in the amount of CsBr does not suppress the leakage current or improve the charge injection as observed for incorporating 0D PNCs. In the luminance versus voltage graph of Figure 5b, the turn-on voltage is increased for 2:1 and 3:1 precursor films, and the peak luminance is lowered relative to the 1.5:1 3D-only phase. The EQE versus voltage plot (Figure 5b, inset) shows that the EQE peak values fall from 2.7% for the 3D-only device to 2.5% for the 2:1 phase and 2.3% for the 3:1 phase. Thus, the spontaneous 0D phase formation from higher CsBr:PbBr₂ precursor formulations does not benefit device performance in our case, likely due to their nonluminescent nature. This lowered performance highlights the contrasting improved light-emitting performance of 3D–0D composite originating from our pre-synthesized PNCs compared to the typical approach of previous literature reports.

3. Conclusion

We have demonstrated that incorporation of an optimized amount of highly emissive 0D Cs₄PbBr₆ PNCs into 3D CsPbBr₃ PeLECs using a novel solvent engineering method dramatically improves the maximum luminance (11 200 cd m⁻²), power efficiency (33.0 lm W⁻¹), and quantum efficiency (8.3%), as well as the operational stability (129 h at 10 mA cm⁻²) of the device. This operational stability is among the best for perovskite electroluminescent devices. It also improves the film morphology by reducing grain size, surface roughness, and the number of pinholes, resulting in suppressed leakage current. Contrary to all the previous reports of light-emitting devices involving 3D CsPbBr₃–0D Cs₄PbBr₆ materials where non-emissive 0D part acts mostly as a surface passivating matrix to provide quantum/dielectric confinement, the high intrinsic luminescence of the 0D PNCs plays a crucial role in significantly enhancing the luminance of our composites. This approach opens numerous

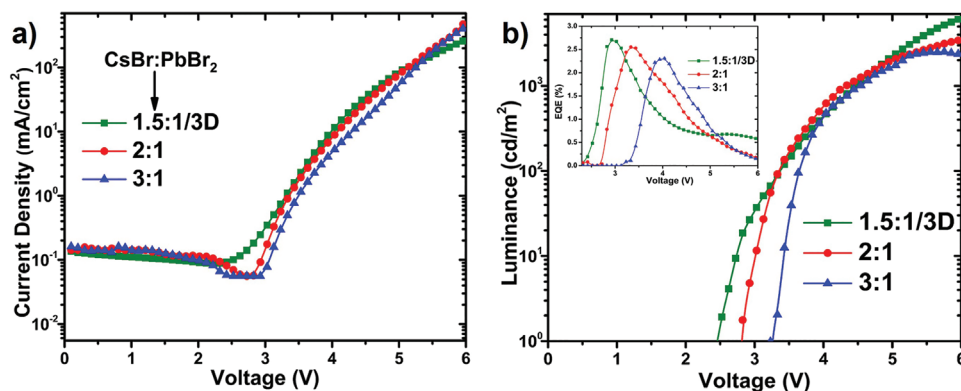


Figure 5. Luminance–current–voltage characteristics of PeLECs formed from different CsBr:PbBr₂ precursor ratios. a) Current density versus voltage for PeLECs formed from different CsBr:PbBr₂ precursor ratios. b) Luminance versus voltage for PeLECs formed from different CsBr:PbBr₂ precursor ratios. (Inset: EQE vs voltage for PeLECs formed from different CsBr:PbBr₂ precursor ratios.)

avenues to explore 0D Cs_4PbBr_6 PNCs for high-performance electroluminescent devices.

4. Experimental Section

Materials: Cesium bromide (CsBr ; 99.99%) and polyethylene oxide (PEO; M.W. > 5 000 000) were purchased from Alfa Aesar. Cesium carbonate (Cs_2CO_3 , 99%), lead bromide (PbBr_2 , >98%), oleic acid (OA, 90%), oleylamine (OLA, 90%), *N,N*-dimethylformamide (DMF, 99.8%), 1,2-dichlorobenzene (DCB, anhydrous, 99%), *n*-hexane (anhydrous, 99.98%), 1-ctadecene (ODE, 90%), lead (II) bromide (PbBr_2 ; 99.99% trace metal basis), lithium hexafluorophosphate (LiPF_6 ; 99.99%), and DMSO (anhydrous > 99.9%) were purchased from Sigma Aldrich. ITO-coated glass slides were purchased from Thin Film Devices, Inc. (Anaheim, CA). Aluminum (99.99%) was purchased from Kurt J. Lesker. LiF was purchased from Sigma Aldrich.

Synthesis of Emissive Cs_4PbBr_6 PNCs: Emissive Cs_4PbBr_6 PNCs were synthesized using reverse microemulsion method.^[9c] In a typical procedure, the PbBr_2 precursor and the Cs-oleate precursor were synthesized separately. First, a mixture of 2.25 g of Cs_2CO_3 and 21.5 mL of OA were stirred and degassed at 130 °C under vacuum for 1 h to generate a yellowish stock of Cs-oleate precursor. Second, 0.2 mL Cs-oleate precursor, 10 mL *n*-hexane, 5 mL OA were loaded in a 50 mL three-neck flask, followed by mild degassing and nitrogen purging. Third, into the flask, a mixture of PbBr_2 (0.03 M, DMF, 1 mL), HBr (48 wt%, 15 μL), 0.1 mL OA, and 0.05 mL OLA was swiftly injected under vigorous stirring. A color change from pale-white to green was observed in 10 min, suggesting the formation of Cs_4PbBr_6 PNCs. The HBr amount was varied to achieve PNCs with different PLQY.^[9d] The as-synthesized nanocrystals were collected via centrifugation at 8000 rpm for 3 min (one-centrifugation-only purification process), followed by dispersion in 2 mL of toluene for further characterization.

Synthesis of Non-Emissive Cs_4PbBr_6 PNCs: Non-emissive Cs_4PbBr_6 PNCs were synthesized following a literature-reported procedure.^[7b] In a typical synthesis, PbBr_2 (0.1 mmol) was dissolved in 5 mL ODE, 0.2 mL OA, and 1.5 mL OLA in a 20 mL vial on a hotplate set at 150 °C. After the PbBr_2 was completely dissolved (around 100 °C), the vial was allowed to cool. When the temperature reached 80 °C, 0.75 mL of Cs-OA (0.4 g Cs_2CO_3 dissolved in 8 mL OA in a 20 mL vial on a hotplate set to 150 °C) was swiftly injected. After about 30 s, the mixture turned turbid white and the vial was quickly cooled down after 8 min to room temperature by immersion in a cold water bath. The PNCs were directly washed by centrifugation (at 4500 rpm for 10 min), followed by redispersion in 6 mL toluene for further characterizations.

Solution Preparation: The CsPbBr_3 precursor solution was prepared by dissolving $\text{CsBr}:\text{PbBr}_2$ in various molar ratios (ranging from 1.5:1 to 3:1) in DMSO and kept overnight for dissolution. PEO (10 mg mL^{-1}) was dissolved in DMSO. The CsPbBr_3 and PEO solutions were mixed in a 5:4 weight ratio. LiPF_6 salt (4 mg mL^{-1} in DMSO) was added to this solution in a 0.5% weight ratio.

Device Fabrication: The ITO/glass substrates ($\approx 20 \Omega \text{ sq}^{-1}$) were cleaned in a sequence of nonionic detergent wash, water bath sonication, and UV ozone treatment. Aqueous PEDOT:PSS solutions (1.3–1.7%, Clevios AI 4083) were filtered through a 0.45 μm GHP filter and then spin-coated to obtain a ≈ 20 nm-thick film on the ITO-coated glass substrates. These films were subsequently annealed at 100 °C for 10 min in a dry N_2 -filled glovebox. The prepared active layer precursor solution was spin cast onto the PEDOT:PSS layer at 1500 rpm for 75 s, and after this time most of the DMSO was rinsed off from the 3D spin-coated films. Dispersed 0D PNCs in HFE (3M Novec 7500, 6–15 mg mL^{-1}) were introduced after 75 s of spin coating and allowed to rest for 10 s for proper mixing of 0D PNCs into 3D matrix followed by 30 s spin coating at 2000 rpm. The spin-coated 3D–0D film was vacuum treated for 150 s to allow all the solvents to be evaporated and then thermally annealed at 150 °C for 35 s to obtain a crystalline 3D–0D thin film. The active layer thicknesses were generally 125–130 nm. To deposit

the top electrode, samples were transferred to a vacuum chamber, and 10 Å LiF and 800 Å Al were deposited using a shadow mask that defined 12 devices per substrate, each with a 3 mm^2 device area.

EL Measurements: The current–voltage electrical characteristics were obtained with a 760D electrochemical analyzer from CH Instruments (Austin, TX), with radiant exitance measurements acquired with a calibrated Labsphere integrating sphere equipped with a thermoelectric-cooled silicon photodetector and Keithley 6485 picoammeter. Each cyclic LIV sweep was performed at 0.1 V s^{-1} with 5 s of interval between each scan. EL spectra were measured with an Ocean Optics Jazz fiber spectrometer. Lifetime measurements were obtained with a custom multiplexer testing station capable of measuring 16 light-emitting devices simultaneously. In brief, this instrument supplied constant current and measured voltage with custom circuitry and simultaneously captured radiant flux with a calibrated Hamamatsu photodiode (S2387-1010R) for each device.

SEM: Secondary-electron SEM images were taken with a Zeiss Supra-40 SEM using an in-lens detector at an accelerating voltage of 10 kV.

AFM: The AFM images were taken using a Veeco Model 3100 Dimension V to scrutinize the morphology of thin films. The thin films were scanned for 5 $\mu\text{m} \times 5 \mu\text{m}$ area at 0.8 Hz rate using an OTESPA-R3 AFM tip from Bruker. Tapping-mode AFM was used for this characterization.

XRD: XRD measurements were collected using a Rigaku SmartLab X-ray Cu target ($K_{\alpha} = 1.5418 \text{ \AA}$) and a HyPix 3000 detector. The $2\theta/\omega$ scan was consistently performed in the 2θ range of 10° to 55° with a 0.01° step and an $\approx 1^\circ \text{ min}^{-1}$ scan speed.

HRTEM: Low-dose HRTEM images were acquired with a Gatan K2 Summit direct-detection electron-counting (DDEC) camera on a Cs-corrected Titan cubed G2 60–300 electron microscope at 300 kV. A stack of successive short-exposure frames (0.05 s frame $^{-1}$, and 120 frames) was recorded on each particle at extremely low doses ($\approx 30\text{--}40 \text{ e \AA}^{-2}$). Drift between frames was corrected based on literature methods.^[25]

Statistical Analysis: Statistical analysis of PeLEC maximum luminance and EQE was performed and plotted in Figure S2, Supporting Information. No pre-processing of data was performed. Data was presented as the mean \pm standard deviation for $n = 12$ devices. A two-tailed *t*-test was performed with Excel, and *p* values were reported.

Supporting Information

Supporting Information is available from the Wiley Online Library or from the author.

Acknowledgements

A.M. and R.B. contributed equally to this work. J.D.S. acknowledges support from the National Science Foundation (ECCS 1906505). R.B., Y.Z., and A.V.M. were supported by the U.S. Department of Energy, Office of Basic Energy Sciences, Division of Materials Sciences and Engineering (DE-SC0010697). W.X. and J.W.P.H. acknowledge the support of Texas Instruments Distinguished Chair of Nanoelectronics. The authors thank Kepeng Song of Shandong University for assistance with the HRTEM.

Conflict of Interest

The authors declare no conflict of interest.

Data Availability Statement

The data that support the findings of this study are available from the corresponding author upon reasonable request.

Keywords

0D–3D composites, Cs₄PbBr₆ nanocrystals, electroluminescence, light-emitting electrochemical cells, perovskites

Received: April 10, 2022

Revised: June 6, 2022

Published online:

- [1] a) M. M. Lee, J. Teuscher, T. Miyasaka, T. N. Murakami, H. J. Snaith, *Science* **2012**, 338, 643; b) M. Liu, M. B. Johnston, H. J. Snaith, *Nature* **2013**, 501, 395; c) J. H. Heo, S. H. Im, J. H. Noh, T. N. Mandal, C.-S. Lim, J. A. Chang, Y. H. Lee, H.-J. Kim, A. Sarkar, M. K. Nazeeruddin, M. Grätzel, S. I. Seok, *Nat. Photonics* **2013**, 7, 486; d) N. J. Jeon, J. H. Noh, Y. C. Kim, W. S. Yang, S. Ryu, S. I. Seok, *Nat. Mater.* **2014**, 13, 897; e) F. Deschler, M. Price, S. Pathak, L. E. Klintberg, D.-D. Jarausch, R. Higler, S. Hüttner, T. Leijtens, S. D. Stranks, H. J. Snaith, M. Atatüre, R. T. Phillips, R. H. Friend, *J. Phys. Chem. Lett.* **2014**, 5, 1421; f) Z.-K. Tan, R. S. Moghaddam, M. L. Lai, P. Docampo, R. Higler, F. Deschler, M. Price, A. Sadhanala, L. M. Pazos, D. Credgington, F. Hanusch, T. Bein, H. J. Snaith, R. H. Friend, *Nat. Nanotechnol.* **2014**, 9, 687; g) S. D. Stranks, H. J. Snaith, *Nat. Nanotechnol.* **2015**, 10, 391; h) F. Meinardi, Q. A. Akkerman, F. Bruni, S. Park, M. Mauri, Z. Dang, L. Manna, S. Brovelli, *ACS Energy Lett.* **2017**, 2, 2368; i) I. Dursun, C. Shen, M. R. Parida, J. Pan, S. P. Sarmah, D. Priante, N. Alyami, J. Liu, M. I. Saidaminov, M. S. Alias, A. L. Abdelhady, T. K. Ng, O. F. Mohammed, B. S. Ooi, O. M. Bakr, *ACS Photonics* **2016**, 3, 1150; j) D. N. Congreve, M. C. Weidman, M. Seitz, W. Paritmongkol, N. S. Dahod, W. A. Tisdale, *ACS Photonics* **2017**, 4, 476; k) H. Wang, D. H. Kim, *Chem. Soc. Rev.* **2017**, 46, 5204.
- [2] a) L. Protesescu, S. Yakunin, M. I. Bodnarchuk, F. Krieg, R. Caputo, C. H. Hendon, R. X. Yang, A. Walsh, M. V. Kovalenko, *Nano Lett.* **2015**, 15, 3692; b) N. Yantara, S. Bhaumik, F. Yan, D. Sabba, H. A. Dewi, N. Mathews, P. P. Boix, H. V. Demir, S. Mhaisalkar, *J. Phys. Chem. Lett.* **2015**, 6, 4360; c) X. Li, Y. Wu, S. Zhang, B. Cai, Y. Gu, J. Song, H. Zeng, *Adv. Funct. Mater.* **2016**, 26, 2435; d) Y. Tong, E. Bladt, M. F. Aygüler, A. Manzi, K. Z. Milowska, V. A. Hintermayr, P. Docampo, S. Bals, A. S. Urban, L. Polavarapu, J. Feldmann, *Angew. Chem., Int. Ed.* **2016**, 55, 13887; e) J. Song, J. Li, X. Li, L. Xu, Y. Dong, H. Zeng, *Adv. Mater.* **2015**, 27, 7162; f) A. Swarnkar, R. Chulliyil, V. K. Ravi, M. Irfanullah, A. Chowdhury, A. Nag, *Angew. Chem., Int. Ed.* **2015**, 54, 15424; g) G. Li, F. W. R. Rivaola, N. J. L. K. Davis, S. Bai, T. C. Jellicoe, F. de la Peña, S. Hou, C. Ducati, F. Gao, R. H. Friend, N. C. Greenham, Z.-K. Tan, *Adv. Mater.* **2016**, 28, 3528; h) X. Zhang, C. Sun, Y. Zhang, H. Wu, C. Ji, Y. Chuai, P. Wang, S. Wen, C. Zhang, W. W. Yu, *J. Phys. Chem. Lett.* **2016**, 7, 4602; i) J. Si, Y. Liu, Z. He, H. Du, K. Du, D. Chen, J. Li, M. Xu, H. Tian, H. He, D. Di, C. Lin, Y. Cheng, J. Wang, Y. Jin, *ACS Nano* **2017**, 11, 11100; j) E. Yassitepe, Z. Yang, O. Voznyy, Y. Kim, G. Walters, J. A. Castañeda, P. Kanjanaboos, M. Yuan, X. Gong, F. Fan, J. Pan, S. Hoogland, R. Comin, O. M. Bakr, L. A. Padilha, A. F. Nogueira, E. H. Sargent, *Adv. Funct. Mater.* **2016**, 26, 8757; k) Y. Shen, L.-P. Cheng, Y.-Q. Li, W. Li, J.-D. Chen, S.-T. Lee, J.-X. Tang, *Adv. Mater.* **2019**, 31, 1901517; l) Y.-K. Wang, F. Yuan, Y. Dong, J.-Y. Li, A. Johnston, B. Chen, M. I. Saidaminov, C. Zhou, X. Zheng, Y. Hou, K. Bertens, H. Ebe, D. Ma, Z. Deng, S. Yuan, R. Chen, L. K. Sagar, J. Liu, J. Fan, P. Li, X. Li, Y. Gao, M.-K. Fung, Z.-H. Lu, O. M. Bakr, L.-S. Liao, E. H. Sargent, *Angew. Chem., Int. Ed.* **2021**, 60, 16164.
- [3] a) K. B. Lin, J. Xing, L. N. Quan, F. P. G. de Arquer, X. W. Gong, J. X. Lu, L. Q. Xie, W. J. Zhao, D. Zhang, C. Z. Yan, W. Q. Li, X. Y. Liu, Y. Lu, J. Kirman, E. H. Sargent, Q. H. Xiong, Z. H. Wei, *Nature* **2018**, 562, 245; b) L. N. Quan, B. P. Rand, R. H. Friend, S. G. Mhaisalkar, T. W. Lee, E. H. Sargent, *Chem. Rev.* **2019**, 119, 7444; c) Y. Cao, N. Wang, H. Tian, J. Guo, Y. Wei, H. Chen, Y. Miao, W. Zou, K. Pan, Y. He, H. Cao, Y. Ke, M. Xu, Y. Wang, M. Yang, K. Du, Z. Fu, D. Kong, D. Dai, Y. Jin, G. Li, H. Li, Q. Peng, J. Wang, W. Huang, *Nature* **2018**, 562, 249; d) B. Zhao, Y. Lian, L. Cui, G. Divitini, G. Kusch, E. Ruggeri, F. Auras, W. Li, D. Yang, B. Zhu, R. A. Oliver, J. L. MacManus-Driscoll, S. D. Stranks, D. Di, R. H. Friend, *Nat. Electron.* **2020**, 3, 704; e) H. C. Cho, S. H. Jeong, M. H. Park, Y. H. Kim, C. Wolf, C. L. Lee, J. H. Heo, A. Sadhanala, N. Myoung, S. Yoo, S. H. Im, R. H. Friend, T. W. Lee, *Science* **2015**, 350, 1222; f) Z. Fang, W. Chen, Y. Shi, J. Zhao, S. Chu, J. Zhang, Z. Xiao, *Adv. Funct. Mater.* **2020**, 30, 1909754; g) Y.-H. Kim, S. Kim, A. Kakekhani, J. Park, J. Park, Y.-H. Lee, H. Xu, S. Nagane, R. B. Wexler, D.-H. Kim, S. H. Jo, L. Martínez-Sarti, P. Tan, A. Sadhanala, G.-S. Park, Y.-W. Kim, B. Hu, H. J. Bolink, S. Yoo, R. H. Friend, A. M. Rappe, T.-W. Lee, *Nat. Photonics* **2021**, 15, 148; h) T. Chiba, Y. Hayashi, H. Ebe, K. Hoshi, J. Sato, S. Sato, Y.-J. Pu, S. Ohisa, J. Kido, *Nat. Photonics* **2018**, 12, 681; i) X. Zhao, Z.-K. Tan, *Nat. Photonics* **2020**, 14, 215.
- [4] a) Y. Dong, Y.-K. Wang, F. Yuan, A. Johnston, Y. Liu, D. Ma, M.-J. Choi, B. Chen, M. Chekini, S.-W. Baek, L. K. Sagar, J. Fan, Y. Hou, M. Wu, S. Lee, B. Sun, S. Hoogland, R. Quintero-Bermudez, H. Ebe, P. Todorovic, F. Dinic, P. Li, H. T. Kung, M. I. Saidaminov, E. Kumacheva, E. Spiecker, L.-S. Liao, O. Voznyy, Z.-H. Lu, E. H. Sargent, *Nat. Nanotechnol.* **2020**, 15, 668; b) C. Wu, Y. Zou, T. Wu, M. Ban, V. Pecunia, Y. Han, Q. Liu, T. Song, S. Duhm, B. Sun, *Adv. Funct. Mater.* **2017**, 27, 1700338; c) D. Yang, X. Li, H. Zeng, *Adv. Mater. Interfaces* **2018**, 5, 1701662; d) R. Grisorio, M. E. Di Clemente, E. Fanizza, I. Allegretta, D. Altamura, M. Striccoli, R. Terzano, C. Giannini, M. Irimia-Vladu, G. P. Suranna, *Nanoscale* **2019**, 11, 986.
- [5] a) K. Lin, J. Xing, L. N. Quan, F. P. G. de Arquer, X. Gong, J. Lu, L. Xie, W. Zhao, D. Zhang, C. Yan, W. Li, X. Liu, Y. Lu, J. Kirman, E. H. Sargent, Q. Xiong, Z. Wei, *Nature* **2018**, 562, 245; b) J. Song, J. Li, L. Xu, J. Li, F. Zhang, B. Han, Q. Shan, H. Zeng, *Adv. Mater.* **2018**, 30, 1800764; c) P. Liu, W. Chen, W. Wang, B. Xu, D. Wu, J. Hao, W. Cao, F. Fang, Y. Li, Y. Zeng, R. Pan, S. Chen, W. Cao, X. W. Sun, K. Wang, *Chem. Mater.* **2017**, 29, 5168; d) W. Cai, Z. Chen, D. Chen, S. Su, Q. Xu, H.-L. Yip, Y. Cao, *RSC Adv.* **2019**, 9, 27684; e) Y.-K. Wang, D. Ma, F. Yuan, K. Singh, J. M. Pina, A. Johnston, Y. Dong, C. Zhou, B. Chen, B. Sun, H. Ebe, J. Fan, M.-J. Sun, Y. Gao, Z.-H. Lu, O. Voznyy, L.-S. Liao, E. H. Sargent, *Nat. Commun.* **2020**, 11, 3674; f) S. Zou, Y. Liu, J. Li, C. Liu, R. Feng, F. Jiang, Y. Li, J. Song, H. Zeng, M. Hong, X. Chen, *J. Am. Chem. Soc.* **2017**, 139, 11443; g) X. Zhou, Y. Zhao, W. Huang, Y. Wu, Z. Wu, G. He, *Org. Electron.* **2021**, 96, 106253; h) J. Song, T. Fang, J. Li, L. Xu, F. Zhang, B. Han, Q. Shan, H. Zeng, *Adv. Mater.* **2018**, 30, 1805409; i) H. Wang, X. Zhang, Q. Wu, F. Cao, D. Yang, Y. Shang, Z. Ning, W. Zhang, W. Zheng, Y. Yan, S. V. Kershaw, L. Zhang, A. L. Rogach, X. Yang, *Nat. Commun.* **2019**, 10, 665; j) J. Li, L. Xu, T. Wang, J. Song, J. Chen, J. Xue, Y. Dong, B. Cai, Q. Shan, B. Han, H. Zeng, *Adv. Mater.* **2017**, 29, 1603885; k) C. Sun, Y. Zhang, C. Ruan, C. Yin, X. Wang, Y. Wang, W. W. Yu, *Adv. Mater.* **2016**, 28, 10088.
- [6] a) M. I. Saidaminov, O. F. Mohammed, O. M. Bakr, *ACS Energy Lett.* **2017**, 2, 889; b) J. Almutlaq, J. Yin, O. F. Mohammed, O. M. Bakr, *J. Phys. Chem. Lett.* **2018**, 9, 4131; c) P. Arunkumar, H. B. Cho, K. H. Gil, S. Unithrattil, Y. H. Kim, W. Bin Im, *Nat. Commun.* **2018**, 9, 4691; d) Q. A. Akkerman, A. L. Abdelhady, L. Manna, *J. Phys. Chem. Lett.* **2018**, 9, 2326.
- [7] a) L. Wu, H. Hu, Y. Xu, S. Jiang, M. Chen, Q. Zhong, D. Yang, Q. Liu, Y. Zhao, B. Sun, Q. Zhang, Y. Yin, *Nano Lett.* **2017**, 17, 5799; b) F. Palazon, C. Urso, L. De Trizio, Q. Akkerman, S. Marras, F. Locardi, I. Nelli, M. Ferretti, M. Prato, L. Manna, *ACS Energy Lett.* **2017**, 2, 2445; c) M. Shin, S.-W. Nam, A. Sadhanala, R. Shivanna,

- M. Anaya, A. Jiménez-Solano, H. Yoon, S. Jeon, S. D. Stranks, R. L. Z. Hoye, B. Shin, *ACS Appl. Energy Mater.* **2020**, *3*, 192; d) Q. A. Akkerman, S. Park, E. Radicchi, F. Nunzi, E. Mosconi, F. De Angelis, R. Brescia, P. Rastogi, M. Prato, L. Manna, *Nano Lett.* **2017**, *17*, 1924; e) D. Han, H. Shi, W. Ming, C. Zhou, B. Ma, B. Saparov, Y.-Z. Ma, S. Chen, M.-H. Du, *J. Mater. Chem. C* **2018**, *6*, 6398; f) Z. Qin, S. Dai, V. G. Hadjiev, C. Wang, L. Xie, Y. Ni, C. Wu, G. Yang, S. Chen, L. Deng, Q. Yu, G. Feng, Z. M. Wang, J. Bao, *Chem. Mater.* **2019**, *31*, 9098; g) N. Riesen, M. Lockrey, K. Badek, H. Riesen, *Nanoscale* **2019**, *11*, 3925.
- [8] a) S. Seth, A. Samanta, *J. Phys. Chem. Lett.* **2017**, *8*, 4461; b) M. De Bastiani, I. Dursun, Y. Zhang, B. A. Alshankiti, X.-H. Miao, J. Yin, E. Yengel, E. Alarousu, B. Turedi, J. M. Almutlaq, M. I. Saidaminov, S. Mitra, I. Gereige, A. AlSaggaf, Y. Zhu, Y. Han, I. S. Roqan, J.-L. Bredas, O. F. Mohammed, O. M. Bakr, *Chem. Mater.* **2017**, *29*, 7108; c) S. Seth, A. Samanta, *J. Phys. Chem. Lett.* **2018**, *9*, 176; d) J. Yin, P. Maity, M. De Bastiani, I. Dursun, O. M. Bakr, J.-L. Brédas, O. F. Mohammed, *Sci. Adv.* **2017**, *3*, e1701793; e) P. Pal, S. Saha, A. Banik, A. Sarkar, K. Biswas, *Chem. – Eur. J.* **2018**, *24*, 1811; f) H. Zhang, Q. Liao, Y. Wu, J. Chen, Q. Gao, H. Fu, *Phys. Chem. Chem. Phys.* **2017**, *19*, 29092; g) Y.-K. Jung, J. Calbo, J.-S. Park, L. D. Whalley, S. Kim, A. Walsh, *J. Mater. Chem. A* **2019**, *7*, 20534; h) M. Hu, C. Ge, J. Yu, J. Feng, *J. Phys. Chem. C* **2017**, *121*, 27053.
- [9] a) M. I. Saidaminov, J. Almutlaq, S. Sarmah, I. Dursun, A. A. Zhumeikenov, R. Begum, J. Pan, N. Cho, O. F. Mohammed, O. M. Bakr, *ACS Energy Lett.* **2016**, *1*, 840; b) D. Chen, Z. Wan, X. Chen, Y. Yuan, J. Zhong, *J. Mater. Chem. C* **2016**, *4*, 10646; c) Y. Zhang, M. I. Saidaminov, I. Dursun, H. Yang, B. Murali, E. Alarousu, E. Yengel, B. A. Alshankiti, O. M. Bakr, O. F. Mohammed, *J. Phys. Chem. Lett.* **2017**, *8*, 961; d) J. Yin, H. Yang, K. Song, A. M. El-Zohry, Y. Han, O. M. Bakr, J.-L. Brédas, O. F. Mohammed, *J. Phys. Chem. Lett.* **2018**, *9*, 5490; e) J. Zhang, A. Wang, L. Kong, L. Zhang, Z. Deng, *J. Alloys Compd.* **2019**, *797*, 1151; f) Y. Zhang, L. Sinatra, E. Alarousu, J. Yin, A. M. El-Zohry, O. M. Bakr, O. F. Mohammed, *J. Phys. Chem. C* **2018**, *122*, 6493; g) Y. Zhang, T. Guo, H. Yang, R. Bose, L. Liu, J. Yin, Y. Han, O. M. Bakr, O. F. Mohammed, A. V. Malko, *Nat. Commun.* **2019**, *10*, 2930.
- [10] a) L. N. Quan, R. Quintero-Bermudez, O. Voznyy, G. Walters, A. Jain, J. Z. Fan, X. Zheng, Z. Yang, E. H. Sargent, *Adv. Mater.* **2017**, *29*, 1605945; b) Z. Bao, H.-D. Chiu, W. Wang, Q. Su, T. Yamada, Y.-C. Chang, S. Chen, Y. Kanemitsu, R.-J. Chung, R.-S. Liu, *J. Phys. Chem. Lett.* **2020**, *11*, 10196; c) Z. Bao, Y.-J. Tseng, W. You, W. Zheng, X. Chen, S. Mahlik, A. Lazarowska, T. Lesniewski, M. Grinberg, C. Ma, W. Sun, W. Zhou, R.-S. Liu, J. P. Attfield, *J. Phys. Chem. Lett.* **2020**, *11*, 7637; d) M. He, C. Wang, J. Li, J. Wu, S. Zhang, H.-C. Kuo, L. Shao, S. Zhao, J. Zhang, F. Kang, G. Wei, *Nanoscale* **2019**, *11*, 22899; e) W. Wang, D. Wang, F. Fang, S. Fang, G. Xu, T. Zhang, *Cryst. Growth Des.* **2018**, *18*, 6133; f) L. Xu, J. Li, T. Fang, Y. Zhao, S. Yuan, Y. Dong, J. Song, *Nanoscale Adv.* **2019**, *1*, 980.
- [11] a) Y. Ling, L. Tan, X. Wang, Y. Zhou, Y. Xin, B. Ma, K. Hanson, H. Gao, *J. Phys. Chem. Lett.* **2017**, *8*, 3266; b) G. Jin, D. Zhang, P. Pang, Z. Ye, T. Liu, G. Xing, J. Chen, D. Ma, *J. Mater. Chem. C* **2021**, *9*, 916; c) X. Chen, F. Zhang, Y. Ge, L. Shi, S. Huang, J. Tang, Z. Lv, L. Zhang, B. Zou, H. Zhong, *Adv. Funct. Mater.* **2018**, *28*, 1706567.
- [12] a) C.-Y. Huang, S.-H. Huang, C.-L. Wu, Z.-H. Wang, C.-C. Yang, *ACS Appl. Nano Mater.* **2020**, *3*, 11760; b) Z. Wang, Y. Zhang, X. Liu, Y. Yu, F. Xu, J. Ding, X. Liang, K. Yang, W. Xiang, *Adv. Mater. Technol.* **2021**, *6*, 2100654; c) X. Li, Z. Wen, S. Ding, F. Fang, B. Xu, J. Sun, C. Liu, K. Wang, X. W. Sun, *Adv. Opt. Mater.* **2020**, *8*, 2000232; d) C. Jia, H. Li, X. Meng, H. Li, *Chem. Commun.* **2018**, *54*, 6300.
- [13] J. Xu, W. Huang, P. Li, D. R. Onken, C. Dun, Y. Guo, K. B. Ucer, C. Lu, H. Wang, S. M. Geyer, R. T. Williams, D. L. Carroll, *Adv. Mater.* **2017**, *29*, 1703703.
- [14] a) T. Xuan, S. Lou, J. Huang, L. Cao, X. Yang, H. Li, J. Wang, *Nanoscale* **2018**, *10*, 9840; b) F. Cao, D. Yu, X. Xu, Z. Han, H. Zeng, *J. Phys. Chem. C* **2021**, *125*, 3; c) G. Hu, W. Qin, M. Liu, X. Ren, X. Wu, L. Yang, S. Yin, *J. Mater. Chem. C* **2019**, *7*, 4733.
- [15] a) H. Lian, Y. Li, K. Sharafudeen, W. Zhao, G. R. Krishnan, S. Zhang, J. Qiu, K. Huang, G. Han, *Adv. Mater.* **2020**, *32*, 2002495; b) S. Huang, S. Yang, Q. Wang, R. Wu, Q. Han, W. Wu, *RSC Adv.* **2019**, *9*, 42430; c) Y. Wang, D. Yu, Z. Wang, X. Li, X. Chen, V. Nalla, H. Zeng, H. Sun, *Small* **2017**, *13*, 1701587; d) F. Cao, D. Yu, W. Ma, X. Xu, B. Cai, Y. M. Yang, S. Liu, L. He, Y. Ke, S. Lan, K.-L. Choy, H. Zeng, *ACS Nano* **2020**, *14*, 5183; e) Z. Bao, J.-W. Luo, Y.-S. Wang, T.-C. Hu, S.-Y. Tsai, Y.-T. Tsai, H.-C. Wang, F.-H. Chen, Y.-C. Lee, T.-L. Tsai, R.-J. Chung, R.-S. Liu, *Chem. Eng. J.* **2021**, *426*, 130849; f) X. Lian, X. Wang, Y. Ling, E. Lochner, L. Tan, Y. Zhou, B. Ma, K. Hanson, H. Gao, *Adv. Funct. Mater.* **2019**, *29*, 1807345; g) Q. Wang, W. Wu, R. Wu, S. Yang, Y. Wang, J. Wang, Z. Chai, Q. Han, *Colloid Interface Sci.* **2019**, *554*, 133.
- [16] a) Z. Bao, H.-C. Wang, Z.-F. Jiang, R.-J. Chung, R.-S. Liu, *Inorg. Chem.* **2018**, *57*, 13071; b) H. Zhao, R. Sun, Z. Wang, K. Fu, X. Hu, Y. Zhang, *Adv. Funct. Mater.* **2019**, *29*, 1902262; c) X. Sun, Z. Gao, Y. Liu, Z. Wang, X. Wang, W. Zhang, B. Xu, X. Meng, *ACS Photonics* **2019**, *6*, 3290; d) Y. Liu, X. Sun, Z. Gao, Y. Hou, K. Wang, W. Zhang, Z. Wang, X. Wang, B. Xu, X. Meng, *J. Phys. Chem. C* **2020**, *124*, 25499; e) Y. Li, W. Shao, L. Chen, J. Wang, J. Nie, H. Zhang, S. Zhang, R. Gao, X. Ouyang, X. Ouyang, Q. Xu, *NPG Asia Mater.* **2021**, *13*, 40; f) J. Yang, Z. Liu, F. Zeng, M. Pi, T. Shi, Y. Bian, X. Tang, J. Du, W. Liu, Y. Leng, *Sol. RRL* **2019**, *3*, 1900127.
- [17] a) P. Andricevic, X. Mettan, M. Kollar, B. Nafradi, A. Sienkiewicz, T. Garma, L. Rossi, L. Forro, E. Horvath, *ACS Photonics* **2019**, *6*, 967; b) M. Alahbakhshi, A. Mishra, R. Haroldson, A. Ishteev, J. Moon, Q. Gu, J. D. Slinker, A. A. Zakhidov, *ACS Energy Lett.* **2019**, *4*, 2922; c) A. Mishra, M. Alahbakhshi, R. Haroldson, L. D. Bastatas, Q. Gu, A. A. Zakhidov, J. D. Slinker, *Adv. Opt. Mater.* **2020**, *8*, 2000226; d) A. Mishra, S. DiLuzio, M. Alahbakhshi, A. C. Adams, M. H. Bowler, J. Moon, Q. Gu, A. A. Zakhidov, S. Bernhard, J. D. Slinker, *Chem. Mater.* **2021**, *33*, 1201; e) A. Mishra, M. Alahbakhshi, R. Haroldson, Q. Gu, A. A. Zakhidov, J. D. Slinker, *Adv. Funct. Mater.* **2021**, *31*, 2102006; f) A. Mishra, M. Alahbakhshi, Q. Gu, A. A. Zakhidov, J. D. Slinker, *ACS Mater. Lett.* **2021**, *3*, 1357; g) M. F. Ayguler, M. D. Weber, B. M. D. Puscher, D. D. Medina, P. Docampo, R. D. Costa, *J. Phys. Chem. C* **2015**, *119*, 12047; h) H. M. Zhang, H. Lin, C. J. Liang, H. Liu, J. J. Liang, Y. Zhao, W. G. Zhang, M. J. Sun, W. K. Xiao, H. Li, S. Polizzi, D. Li, F. J. Zhang, Z. Q. He, W. C. H. Choy, *Adv. Funct. Mater.* **2015**, *25*, 7226.
- [18] a) Q. B. Pei, G. Yu, C. Zhang, Y. Yang, A. J. Heeger, *Science* **1995**, *269*, 1086; b) J. C. deMello, *Phys. Rev. B* **2002**, *66*, 235210; c) J. D. Slinker, J. A. DeFranco, M. J. Jaquith, W. R. Silveira, Y. W. Zhong, J. M. Moran-Mirabal, H. G. Craighead, H. D. Abruna, J. A. Marohn, G. G. Malliaras, *Nat. Mater.* **2007**, *6*, 894; d) R. D. Costa, E. Orti, H. J. Bolink, F. Monti, G. Accorsi, N. Armaroli, *Angew. Chem., Int. Ed.* **2012**, *51*, 8178; e) M. H. Bowler, A. Mishra, A. C. Adams, C. L.-D. Blangy, J. D. Slinker, *Adv. Funct. Mater.* **2020**, *30*, 1906715; f) S. Hu, J. Gao, *Adv. Funct. Mater.* **2020**, *30*, 1907003; g) K. Youssef, Y. Li, S. O'Keeffe, L. Li, Q. Pei, *Adv. Funct. Mater.* **2020**, *30*, 1909102; h) E. Nannen, J. Frohliks, S. Gellner, *Adv. Funct. Mater.* **2020**, *30*, 1907349.
- [19] a) A. A. Zakhidov, J.-K. Lee, H. H. Fong, J. A. DeFranco, M. Chatzichristidi, P. G. Taylor, C. K. Ober, G. G. Malliaras, *Adv. Mater.* **2008**, *20*, 3481; b) M. Hasan, S. Venkatesan, D. Lyashenko, J. D. Slinker, A. Zakhidov, *Anal. Chem.* **2017**, *89*, 9649.
- [20] a) A. B. Tamayo, S. Garon, T. Sajoto, P. I. Djurovich, I. M. Tsyba, R. Bau, M. E. Thompson, *Inorg. Chem.* **2005**, *44*, 8723; b) H.-C. Su, C.-C. Wu, F.-C. Fang, K.-T. Wong, *Appl. Phys. Lett.* **2006**, *89*, 261118.

- [21] a) H. Tsai, S. Shrestha, R. A. Vilá, W. Huang, C. Liu, C.-H. Hou, H.-H. Huang, X. Wen, M. Li, G. Wiederrecht, Y. Cui, M. Cotlet, X. Zhang, X. Ma, W. Nie, *Nat. Photonics* **2021**, *15*, 843; b) T. Wu, J. Li, Y. Zou, H. Xu, K. Wen, S. Wan, S. Bai, T. Song, J. A. McLeod, S. Duhm, F. Gao, B. Sun, *Angew. Chem., Int. Ed.* **2020**, *59*, 4099.
- [22] a) B. M. D. Puscher, M. F. Ayguler, P. Docampo, R. D. Costa, *Adv. Energy Mater.* **2017**, *7*, 1602283; b) L. D. Bastatas, M. D. Moore, J. D. Slinker, *ChemPlusChem* **2018**, *83*, 266.
- [23] Y. Liu, S. Tang, J. Fan, E. Gracia-Espino, J. Yang, X. Liu, S. Kera, M. Fahlman, C. Larsen, T. Wågberg, L. Edman, J. Wang, *ACS Appl. Nano Mater.* **2021**, *4*, 1162.
- [24] a) T. G. Liashenko, E. D. Cherotchenko, A. P. Pushkarev, V. Pakštas, A. Naujokaitis, S. A. Khubezhov, R. G. Polozkov, K. B. Agapev, A. A. Zakhidov, I. A. Shelykh, S. V. Makarov, *Phys. Chem. Chem. Phys.* **2019**, *21*, 18930; b) M. Zhang, Z. Zheng, Q. Fu, Z. Chen, J. He, S. Zhang, L. Yan, Y. Hu, W. Luo, *CrystEngComm* **2017**, *19*, 6797; c) T. G. Liashenko, A. P. Pushkarev, A. Naujokaitis, V. Pakštas, M. Franckevičius, A. A. Zakhidov, S. V. Makarov, *Nanomaterials* **2020**, *10*, 1937.
- [25] D. Zhang, Y. Zhu, L. Liu, X. Ying, C.-E. Hsiung, R. Sougrat, K. Li, Y. Han, *Science* **2018**, *359*, 675.